The effect of collector doping on the high-frequency generation in strongly coupled semiconductor superlattice

V. A. Maksimenko[1,2], V. V. Makarov[1,2], A. A. Koronovskii[1,2], K. N. Alekseev[3], A. G. Balanov[3] and A. E. Hramov[1,2]

[1] *REC "Nonlinear Dynamics of Complex Systems", Saratov State Technical University - Politechnicheskaja 77, Saratov 410028, Russia*
[2] *Faculty of Nonlinear Processes, Saratov State University - Astrakhanskaya 83, Saratov, 410012, Russia*
[3] *Department of Physics, Loughborough University - Loughborough LE11 3TU, UK*

Abstract – This letter focuses on the analysis of the spatio-temporal dynamics of charge domains in strongly coupled semiconductor superlattices with the Ohmic emitter and collector contacts. Our numerical simulations, based on the semiclassical approximation of the electron transport, show that the collector doping can dramatically affect the charge dynamics in the semiconductor structure and, therefore, the output AC power. We demonstrate that the appropriately chosen doping of the collector contacts can considerably increase the power of the generated signal.

Introduction. – The development of the compact devices for the generation, amplification and detection of THz radiation is of utmost importance for many areas of science and technology [1,2]. One of the promising approaches in this development is the use of nano- and micro-structures, which include high-frequency transferred-electron devices (TEDs), solid-state lasers and other semiconductor heterostructures [3].

The recent advances in the crystal-growth technologies enabled high-precision control of the properties of the heterostructures, which significantly improved the performance of the semiconductor devices [4]. This promoted the research aimed to optimize the devices design in order to achieve the maximal output of AC power in sub-THz and THz frequency ranges [5,6]. For example, some TEDs, *e.g.* the Gunn diodes, with the linearly graded doping profiles were shown to demonstrate a better performance as compared to the devices with a uniform doping [7]. A more complicated configuration of the doping densities may contain a notch, caused, *e.g.*, by a thin undoped epitaxial layer between the heavily n-type doped cathode contact and the uniformly n-type doped active transport region. It was found out that such doping profile can lead to a drastic increase of the output power [8]. Another way to improve the characteristics of the Gunn devices is

associated with controlling the injection current through the emitter contact. As is shown in ref. [8], the InP Gunn devices with InGaAsP cathode injectors are more efficient in the generation of signals with frequencies up to 200 GHz than similar devices with Ohmic contacts.

We consider another class of TEDs, namely strongly coupled (miniband) semiconductor superlattices [9]. These structures are now of great research interest from the viewpoint of the prospective application for the microwave generation and amplification in a sub-THz/THz frequency range [10–13]. The high-frequency characteristics of the superlattices are determined by both high mobility of the miniband electrons and THz Bloch oscillations, which can be realised in the device. In addition, a high enough electric field applied to the superlattice can lead to a spatio-temporal instability [14], which results in the formation of the areas with high electron density (the charge domains) propagating along the superlattice [15,16]. It was shown that the moving charge domains are able to generate current oscillations with the frequency up to several hundred GHz [17].

The interest in the practical applications of SLs in sub-THz/THz electronics gave rise to the diverse research activity related to the effects of the external and parasitic circuits, fields, contacts, and load lines on charge transport

in SLs [18–20]. In refs. [21–23] it was demonstrated that a tilted magnetic field applied to a miniband SL significantly modifies the IV curves of the devices and enhance both the power and frequency of the generated current oscillations. The possibility to control the charge transport properties of the SL and Gunn devices by manipulation of the emitter boundary condition was discussed in [24,25]. The effects of the doping in the transport region on DC current and electric stability in miniband SLs according to the conventional NL criterion [26,27] were theoretically studied in [28]. Nevertheless, the influence of the contacts properties on the high-frequency current generation in SLs is still poorly understood.

In this paper we study the collective spatio-temporal dynamics of the charge carriers in the GaAs-AlGaAs semiconductor superlattice with the Ohmic emitter and collector. In particular, we investigate how the collector doping density affects the output power of sub-THz current oscillations in the semiconductor superlattices.

Model for space-charge dynamics. – The charge transport in the strongly coupled semiconductor superlattices can be considered within a semiclassical approximation [21,29]. With this, the collective charge dynamics can be described using a self-consistent set of the current continuity equation

$$\frac{\partial n}{\partial t} = -\frac{1}{e}\frac{\partial J}{\partial x} \tag{1}$$

and Poisson equation

$$\frac{\partial^2 \phi}{\partial x^2} = -\frac{e}{\epsilon_0 \epsilon_r}(n - n_0). \tag{2}$$

Here $J(x,t)$, $n(x,t)$, and $\phi(x,t)$ are the spatial distributions of the current density, the volume electron density and the electric potential, respectively; x is the spatial coordinate along the superlattice, and t is the time. Parameter e indicates the electron charge, ϵ_0 and $\epsilon_r = 12.5$ are the absolute and relative permittivities, respectively; n_0 is the n-type doping density, which is equal to $n_D = 3 \times 10^{22}\,\mathrm{m}^{-3}$ for the transport region of the semiconductor structure, and to $n_C^* = 1 \times 10^{23}\,\mathrm{m}^{-3}$ for the contact regions. It is assumed that interminiband tunnelling can be neglected.

Within the drift approximation [30], the current density in the semiconductor structure is given by

$$J = en\frac{\delta \Delta d}{2\hbar}\frac{eFd\tau_{SL}/\hbar}{1 + (eFd\tau_{SL}/\hbar)^2}, \tag{3}$$

where $F(x,t) = -\partial\phi(x,t)/\partial x$ is the electric field along the superlattice, $\Delta = 19.1\,\mathrm{meV}$ is the miniband width, $\tau_{SL} = 250\,\mathrm{fs}$ is the scattering time, $\delta = 0.12$ is a correction coefficient reflecting the contribution of elastic and inelastic scattering events [22], $d = 8.3\,\mathrm{nm}$ —period of the superlattice.
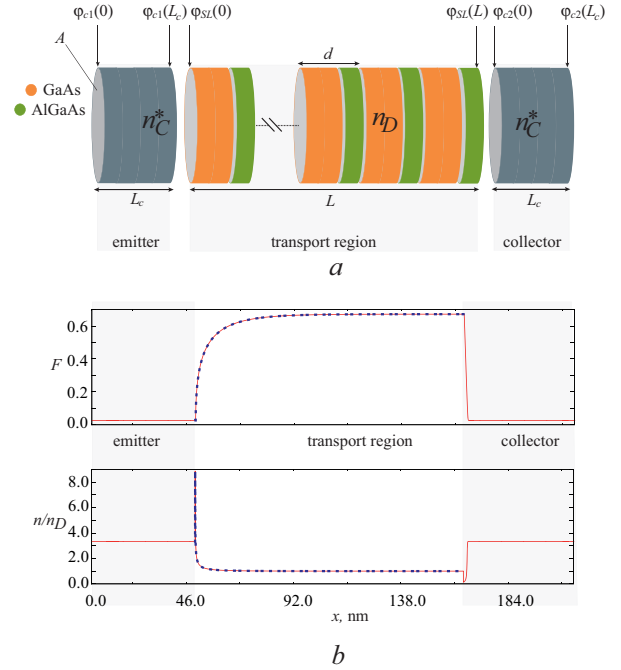

Fig. 1: (Colour on-line) (a) The schematic diagram of the semiconductor superlattice with the highly doped emitter and collector contacts. (b) The spatial distributions of the electric field $F(x)$ and the normalised electron density $n(x)/n_D$ for $V = 0.3\,\mathrm{V}$ and $L = 115.2\,\mathrm{nm}$. The areas of contacts are outlined by the shadow. The distributions $F(x)$ and $n(x)$ corresponding to the transport region are shown by the dotted line.

In the region of the Ohmic emitter and collector the current density J_C is defined according to the Drude model [31]

$$J_C = \frac{e^2 n \tau_C}{m^*}F, \tag{4}$$

where $\tau_C = 90\,\mathrm{fs}$ [32] is the scattering time of the contact material, $m^* = 0.067 m_e$ is the effective mass of the electron. The applied voltage is the global constraint, which is defined by

$$V = \int_0^{L_{SL}} F(x)\mathrm{d}x, \tag{5}$$

where the integration is performed over all the system length $L_{SL} = L + 2L_c$. Here L is the superlattice transport region length and $L_c = 50\,\mathrm{nm}$ is the length of the emitter and collector contacts.

The schematic diagram of the semiconductor superlattice with the Ohmic contacts is shown in fig. 1(a). The functions $\phi_{c1}(x)$, $\phi_{SL}(x)$, and $\phi_{c2}(x)$ correspond to the spatial distributions of the potential along the emitter contact, of the transport region and of the collector contact, respectively. The parameters d and A are the period and the cross-sectional area of the semiconductor structure.

In our calculations we use the following boundary conditions:

$$\phi_{SL}(0) = \phi_{c1}(L_c),$$
$$\phi_{c2}(0) = \phi_{SL}(L),$$
$$J_{SL}(0) = J_{c1}(L_c),$$
$$J_{c2}(0) = J_{SL}(L),$$
(6)

where $J_{SL}(0)$, $J_{c1}(L_c)$, $J_{c2}(0)$, and $J_{SL}(L)$ are the density of the current through the left edge of the superlattice transport region, through the right edge of the emitter, through the left edge of the collector and through the right edge of the transport region, respectively.

Figure 1(b) illustrates a typical stationary spatial distribution of the electric field $F(x)$ and of the normalised electron density. The dependences $F(x)$ and $n(x)/n_D$ in the transport region are indicated by the dotted lines, whereas the same dependences for the contacts are shown by the solid lines. One can see that the equilibrium distribution $F(x)$ in the contacts is highly homogeneous, which can be explained by the linear character of the contact conductivity defined by (4). At the interface between the emitter and the transport region the significant difference between the electron drift velocities leads to the formation of the charge accumulation layer. At the same time, at the interface of the transport region and the collector, a charge depletion layer is formed. Below we show that such accumulation and the depletion layers play a crucial role in the nonequilibrium charge transport.

Effects of the collector doping on the high-frequency generation. – Using the model (1)–(9) we analyse the space-charge dynamics in the GaAs/AlGaAs superlattice with the parameters, which were used in our recent experimental works [22,33,34]. Figure 2(a) depicts the dependence of the normalised power of the current oscillations P/P_0 upon the collector doping density n_C and the length of the superlattice L. The power values P were normalised to the maximal power value P_0 observed within the ranges of n_C and L represented in fig. 2(a). In these calculations the emitter doping density remains constant and equal to n_C^*. The voltage applied to the superlattice was fixed at the value $V = V^* = 0.9\,\text{V}$, for which the charge transport in the superlattice is associated with moving charge domains. The plot in fig. 2(a) demonstrates that the power of the generated current oscillations drops with the increase of the transport region length L. However, there is the optimal collector doping density n_C, for which the power of the oscillations is maximal for the given L. For example, for $L = L^* = 100\,\text{nm}$ (indicated by a dashed line in fig. 2(a), which is close to the length of the superlattices used in recent experiments [22,33], the increase of the collector doping from $n_C^1 = 3.0 \times 10^{22}\,\text{m}^{-3}$ to the optimal value $n_C^2 = 1.0 \times 10^{23}\,\text{m}^{-3}$ evokes an eightfold increase of the generated AC power. With further growth of n_C the oscillations power slowly decreases.

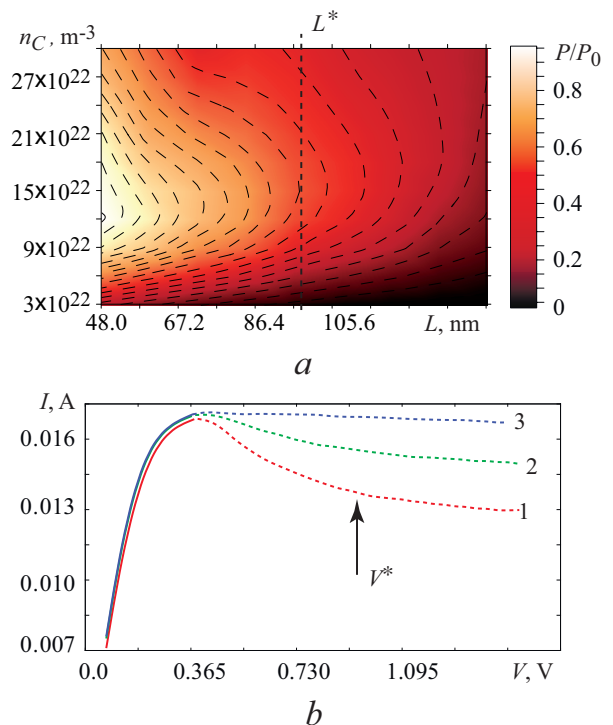The IV curves calculated for different values of the collector doping density are illustrated in fig. 2(b), where

Fig. 2: (Colour on-line) (a) The dependence $P(L_{SL}, n_C)/P_0$ for $V = 0.9\,\text{V}$. (b) The IV curves of the superlattice with the transport region length $L = L^* = 100\,\text{nm}$ (marked by dashed line in (a)) and with $n_C = n_C^1 = 3.0 \times 10^{22}\,\text{m}^{-3}$ (curve 1), $n_C = n_C^2 = 1.0 \times 10^{23}\,\text{m}^{-3}$ (curve 2), $n_C = n_C^3 = 3.0 \times 10^{23}\,\text{m}^{-3}$ (curve 3). The dashed lines show the unstable branches of the IV curves, which correspond to the regime of the moving charge domains. The arrow indicates the voltage $V = 0.9\,\text{V}$, which was fixed for the calculations presented in (a).

curve 1 corresponds to $n_C^1 = 3.0 \times 10^{22}\,\text{m}^{-3}$, curve 2 to $n_C^2 = 1.0 \times 10^{23}\,\text{m}^{-3}$, and curve 3 to $n_C^3 = 3.0 \times 10^{23}\,\text{m}^{-3}$. The graphs evince that, in contrast to the AC power, the DC currents of the superlattice monotonically increase with the growth of the collector doping. Our calculations reveal similar effects of collector doping on DC and AC current for different values of L.

The results discussed above suggest that the collector doping density should have a significant effect of formation and dynamics of charge domains. In order to verify this we consider the dynamics of the spatio-temporal distribution of the electron density $n(t, x)$ along the whole structure, including the emitter, the transport region and the collector (see fig. 1(a)). Figures 3(a), (b), and (c) present the dependences $n(t, x)$ for $L_{SL} = L^*$ and $n_C = n_C^1, n_C^2$, and n_C^3, respectively. Black (white) colour corresponds to high (low) density of electrons. To provide additional illustration of the collective charge dynamics, in figs. 3(d), (e), and (f) we show the log-scaled snapshots of $n(x)$ for different time moments t during one period of currents oscillations. Each snapshot is represented by a curve designated by a number. The larger number correspond to the later moment of time. Figure 3 reveals that, while the
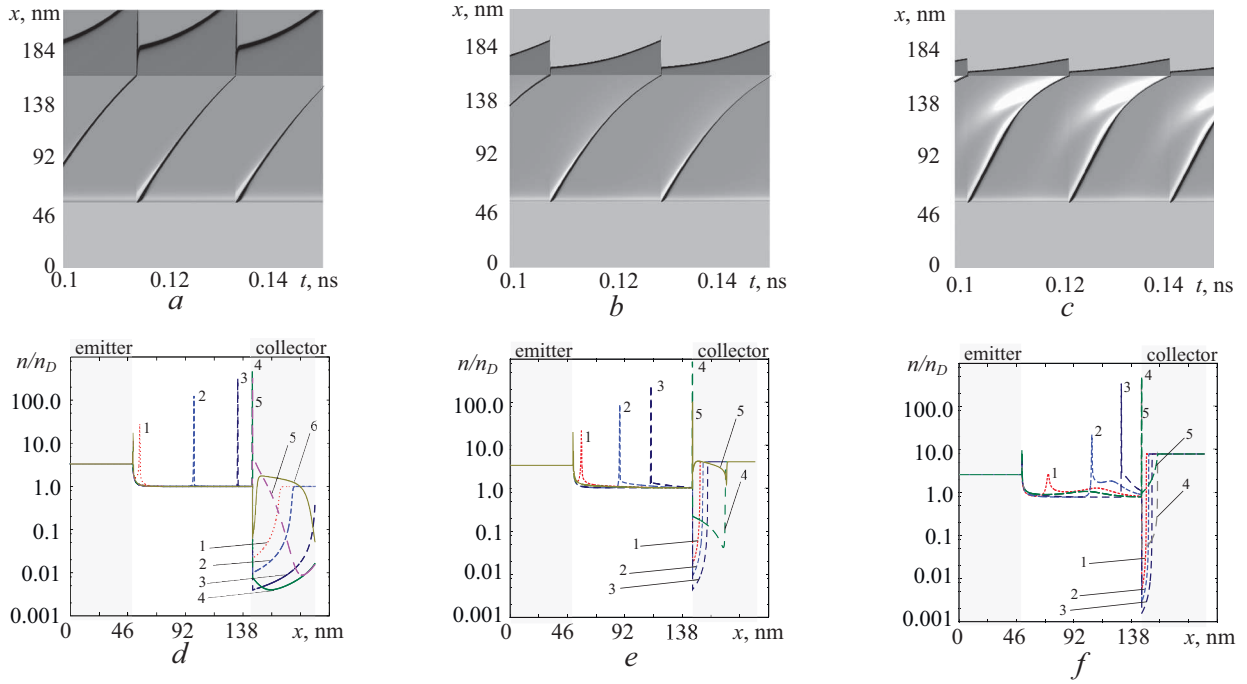
Fig. 3: (Colour on-line) Spatio-temporal dynamics of the charge concentration $n(t,x)$ for (a) $n_C^1 = 3.0 \times 10^{22}\,\mathrm{m}^{-3}$, (b) $n_C^2 = 1.0 \times 10^{23}\,\mathrm{m}^{-3}$, and (c) $n_C^3 = 3.0 \times 10^{23}\,\mathrm{m}^{-3}$. Snapshots of $n(x, t_0)$ for different time moments t_0 within one period of the current oscillations for (d) $n_C^1 = 3.0 \times 10^{22}\,\mathrm{m}^{-3}$, (e) $n_C^2 = 1.0 \times 10^{23}\,\mathrm{m}^{-3}$, and (f) $n_C^3 = 3.0 \times 10^{23}\,\mathrm{m}^{-3}$.

concentration of charge almost everywhere in the emitter remains constant, a domain of high charge concentration appears at the interface of the emitter contact and superlattice transport region (curve 1 in figs. 3(d), (e), (f)). The appearance of this charge domain is compensated by the generation of a depletion region inside collector contact. As the charge domain propagates along the transport region, the concentration of charge inside it grows causing the expanding of the depletion region in the collector (curves 2, 3 in figs. 3(d), (e), (f)). When the domain reaches the collector, it produces a sharp increase of the current, and another charge domain then forms near the emitter. This retrieves the depletion region in the collector (curves 4, 5 in figs. 3(d), (e), (f)), and the domain propagation process repeats producing the current oscillations, whose frequency ranges as 40–50 GHz for the model under consideration.

Notably, the comparison of the graphs in fig. 3 points out that, if the change in the collector doping n_C has almost no effect on the behaviour of the charge concentration in the emitter, it produces a dramatic impact on the dynamics of $n(t, x)$ in the collector contact. For small $n_C = n_C^1 = 3.0 \times 10^{22}\,\mathrm{m}^{-3}$ (figs. 3(a), (d)) the depletion region can occupy the entire length of the collector contact (curves 3, 4 in fig. 3(d)), which produces a large voltage drop along the collector and, as a result, small DC current and AC power generated. The increase of the collector doping up to $n_C^2 = 1.0 \times 10^{23}\,\mathrm{m}^{-3}$ (figs. 3(b), (e)) shrinks the depletion layer in the collector, which leads to growth of both the DC currents and

the AC power. Further increase of n_C up to the value $n_C^3 = 3.0 \times 10^{23}\,\mathrm{m}^{-3}$ (figs. 3(c), (f)) narrows the depletion layer even to a greater extent. However, at the same time, it significantly reshapes the profile of the moving charge domains. As fig. 3(f) shows, in this case the profile $n(x)$ demonstrates two maxima, which expands the domain width, and lowers the charge concentration inside the domain. The expansion of the moving domains increases the DC current through the SL, but low charge concentration inside the domain decreases the amplitude of the current oscillations, and thus the generated AC power.

Conclusion. – In conclusion, we have theoretically studied the influence of the collector doping density on the spatio-temporal charge dynamics in the strongly coupled semiconductor superlattice. Our results demonstrate that, although the collector doping has almost no effect on the charge distribution in the emitter region of the superlattice, it can dramatically affect the formation of the charge accumulation and depletion layers at the interfaces between the transport region and the contacts, and also the evolution of these layers in time. We show that while the increase of the collector doping leads, in general, to the increase of DC current through the superlattice, there is an optimal doping density which corresponds to the maximal AC power generated by the semiconductor superlattice of the given length. This suggests that, in order to maximise the AC power output of the semiconductor superlattice, the collector region should be appropriately doped. Since the model equations used in our

study are applicable to different classes of TEDs, we believe that the results obtained can be useful in the design of a wide range of high-frequency semiconductor superlattices and Gunn diodes.

$* * *$

REFERENCES

[1] TEKAVEC P. F. and KOZLOV V. G., *AIP Conf. Proc.*, **1581** (2014) 1576.

[2] KASHIWAGI T. *et al.*, *Appl. Phys. Lett.*, **104** (2014) 082603.

[3] LU Q. Y. *et al.*, *Appl. Phys. Lett.*, **104** (2014) 221105.

[4] SCHMIDT J. C. *et al.*, *Superlattices Microstruct.*, **52** (2012) 1143.

[5] EISELE H. and HADDAD G. I., *IEEE Trans. Microwave Theory Tech.*, **46** (1998) 739.

[6] EISELE H., RYDBERG A. and HADDAD G. I., *IEEE Trans. Microwave Theory Tech.*, **48** (2000) 626.

[7] EISELE H. and KAMOUA R., *IEEE Trans. Microwave Theory Tech.*, **52** (2004) 2371.

[8] KAMOUA R., *Solid-State Electron.*, **38** (1995) 269.

[9] ESAKI L. and TSU R., *IBM J. Res. Dev.*, **14** (1970) 61.

[10] SHIK A. Y., *Fiz. Tekh. Poluprovodn.*, **8** (1974) 1841 (*Sov. Phys. Semicond.*, **8** (1975) 1195).

[11] TSU R., *Superlattices to Nanoelectronics* (Elsevier, Amsterdam) 2005.

[12] LEI X. *et al.*, *Appl. Phys. Lett.*, **105** (2014) 062112.

[13] BONILLA L. L., ÁLVARO M. and CARRETERO M., *EPL*, **95** (2011) 47001.

[14] BUTIKER M. and THOMAS H., *Phys. Rev. Lett.*, **38** (1977) 78.

[15] RIDLEY B. K., *Proc. Phys. Soc.*, **82** (1963) 954.

[16] KORONOVSKII A. A. *et al.*, *Phys. Rev. B*, **88** (2013) 165304.

[17] SCHOMBURG E. *et al.*, *Appl. Phys. Lett.*, **74** (1999) 2179.

[18] RENK K. F. *et al.*, *Phys. Rev. Lett.*, **95** (2005) 126801.

[19] IGNATOV A. A., *Semicond. Sci. Technol.*, **26** (2011) 055015.

[20] SCHÖLL E., *Nonlinear Spatio-Temporal Dynamics and Chaos in Semiconductors* (Cambridge University Press, Cambridge) 2001.

[21] GREENAWAY M. T. *et al.*, *Phys. Rev. B*, **80** (2009) 205318.

[22] FROMHOLD T. M. *et al.*, *Nature*, **428** (2004) 726.

[23] SELSKII A. O. *et al.*, *Phys. Rev. B*, **84** (2011) 235311.

[24] KROEMER H., *IEEE Trans. Electron Devices*, **ED-15** (1968) 819.

[25] DASCALU D., *J. Appl. Phys.*, **44** (1973) 3609.

[26] SIBILLE A. *et al.*, *Phys. Rev. Lett.*, **64** (1990) 52.

[27] KROEMER H., *Proc. IEEE*, **52** (1964) 1736.

[28] CAO J. C. and LEI X. L., *Phys. Rev. B*, **59** (1999) 2199.

[29] WACKER A., *Phys. Rep.*, **357** (2002) 1.

[30] BALANOV A. G. *et al.*, *JETP*, **114** (2012) 836.

[31] DRUDE P., *Ann. Phys.*, **306** (1900) 566.

[32] HARDWICK D. P. A., *Quantum and semiclassical calculations of electron transport through a stochastic system*, PhD Thesis, School of Physics and Astronomy, University of Nottingham (2007).

[33] HRAMOV A. E. *et al.*, *Phys. Rev. Lett.*, **112** (2014) 116603.

[34] ALEXEEVA N. *et al.*, *Phys. Rev. Lett.*, **109** (2012) 024102.